Focused ion beam milling: Depth control for three-dimensional microfabrication

M. J. Vasile,[a] Z. Niu, R. Nassar, W. Zhang, and S. Liu
Institute for Micromanufacturing, Louisiana Tech University, Ruston, Louisiana 71272

(Received 29 May 1997; accepted 28 July 1997)

Ion milling with a focused ion beam (FIB) is a potential method for making micromolds, which will then be the primary elements in the mass production of micro- or mini-objects by embossing or injection molding. The challenge lies in controlling the ion milling to produce cavities with predefined, arbitrary geometric cross-sections. This work involves programming variations as a function of position into the algorithm that generates the dwell times in the pixel address scheme of a FIB. These variations are done according to whether an axis of symmetry or a plane of symmetry determines the final geometry, and the result is 26 new cross-sectional shapes, such as hemispherical pits, parabolic pits, hemispherical domes, etc. The ion milling control programs were used to generate parabolic cross-section trenches, sinusoidal trenches, sinusoidal cross-section rings on an annulus, and hemispherical domes. We observed reasonable agreement between the shapes ion milled in Si(100) and the expected geometry. The dwell times are generated assuming each pixel has a unique dose and the ion yield is constant with angle of incidence. Deviations from ideality are ascribed to the variation in sputter yield with changing angle of incidence, and to the dwell time control algorithm. Redeposition also compounds the deviation from ideality, but it is difficult to estimate the magnitude of this effect.
[S0734-211X(97)01806-4]

I. INTRODUCTION

A number of applications of focused ion beam (FIB) technology in microelectronics were demonstrated and developed into routine operations for research, and development in the semiconductor industry during the 1980s. Those applications are characteristic of small volume and high value[1] such as direct-write lithography, photomask repair, cross-sectioning of devices,[2] integrated-circuit (IC) reverse engineering/restructuring, maskless implantation, and ion beam assisted etching.[3–5] FIB technologies were extended from their original applications in microelectronic research, and product development to the multidisciplinary area of micromanufacturing for objects with feature sizes in microns in the early 1990s. This departure from photomask repair, reverse engineering, and IC diagnostic applications in the electronics industry to micromachining was stimulated by the promise of FIB milling as a ''direct write'' material removal method,[6,7] which has very few materials restrictions.

Early reports of micromachining for nonelectronic applications have been given by Ishitani *et al.*,[8] where a 45 μm diam microgear was cut in stainless steel foil as a demonstration of feasibility. The applications of FIB for micromachining in Ishitani's initial work, were a demonstration to advocate the vision that FIB is a new and promising high-resolution method for microdevice assembly. Several other applications, such as FIB trimming of a V-shaped cantilever tip for an atomic force microscope (AFM), trimming of a magnetic head, and micromilling of a three-dimensional (3D) copper needle have been demonstrated.[8,9] FIB milling techniques are also being used to produce thin, free-standing membranes that contain specific IC elements for transmission electron microscopy (TEM) of IC structures.[10,11]

A co-axial ion milling process invented at AT&T Bell Labs was used for the routine production of specialized scanning probe microscopy (SPM) tips. The objective was to make a submicron stylus with taper angle and tip radius of curvature within controlled limits. Refinement of the technique has yielded tips which are suitable for the evaluation of SPM as a metrology tool.[12,13] The need to produce specialized tip geometries for probe microscopy applications led to the development of an in-vacuum lathe-type device, which quickly prompted the latest extension of the FIB milling technique to produce a variety of arbitrarily shaped 3D micro-objects and structures.[14,15] The microstructures have potential applications as manipulators for single-cell biological research, microcutters with submicron resolution and micron-sized machine tool bits.[16,17]

This research is intended to expand FIB micromilling capabilities from simple rectangular cross-section or wedge cross-section geometry into nonlinear cross-section geometries, with either an axis or a plane of symmetry that could be used for micromolds and microdevice components. Smoothly curved analog surface geometries are illustrated in Fig. 1. These geometries are representative of the possible elements in designs of micromechanical and micro-optical products. None of these designs can be made on a routine basis by FIB micromachining to date, although some of them have been mathematically studied and experimentally attempted.[18]

The present FIB is a far more versatile tool when the depth variation control capabilities are added to the original ion milling abilities. FIB techniques will become a more so-

[a]Electronic mail: mjv@engr.latech.edu

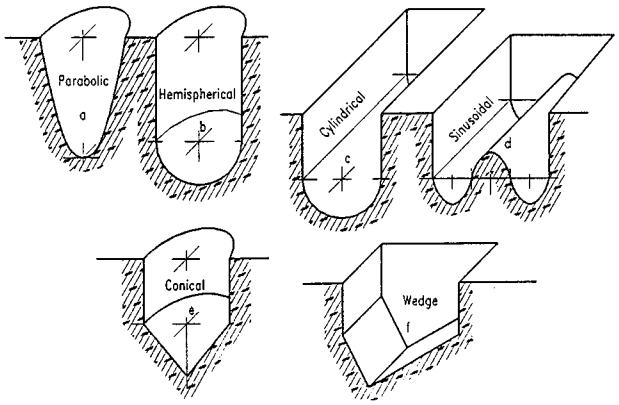

FIG. 1. Representations of 3D cavities for molding or embossing microstructures.

phisticated and refined micromachining method with the addition of depth control, and will be complementary to deep x-ray lithography, microdrilling, microelectrical discharge machining, and laser micromachining technology. These techniques are the next generation of mold and mask fabrications for microelectro-mechanical systems (MEMS), and none of these techniques have a well developed capacity for depth control needed to produce 3D geometry.

A. Programming the ion milling depth control

The control method in this work uses address mode deflection beam writing. The basic scheme of address mode deflection beam writing,[19] is to direct the ion beam onto an object whose surface is sputtered by the ion bombardment. The feature created can be mapped and monitored by digital image formation from ejected secondary electrons. A deflection pattern is also needed, which is stored in another graphic page of memory (image buffer), and can be addressed through the digital image coordinates. The information of the deflection pattern is overlapped onto the selected area of the object, and the ion beam is deflected onto the object surface according to the superimposed pattern information. The ion beam deflection is done point by point with each pixel in the digital image as an address point. The longer the beam dwells on a pixel, the more material is sputtered or machined away at the object location corresponding to the pixel.

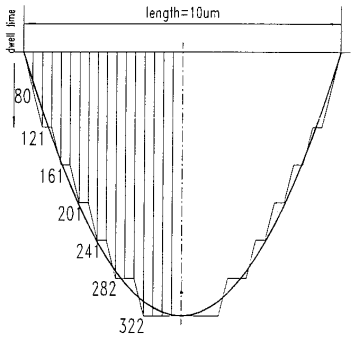

FIG. 2. The profile of the parabolic trough cross-section based on the values of pixel dwell time.

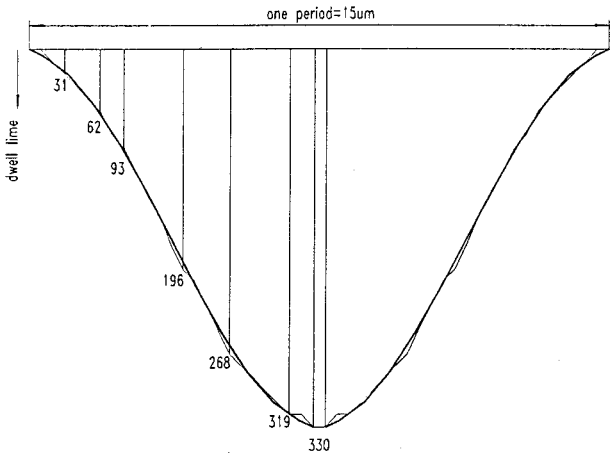

FIG. 3. The profile of the cosine trough cross-section based on the values of pixel dwell time.

Therefore, by controlling the dwell time of the beam for each pixel in the address pattern, we can effect control over the milling depth to realize the type of 3D geometry we desire. The dwell time control technique uses a characteristic length (called the repair length) in the pixel address pattern: a program for pixel dwell time increment and decrement according to the desired geometric function modifies the normally uniform pixel dwell times.

B. Geometric shapes

Parabolic, circular, and sinusoidal geometries have been chosen as the initial shapes for the experimental ion milled cross-sections in this work. The deflection patterns chosen are circles, annulus, and rectangles or squares. The deflection pattern yields either a plane of symmetry or symmetry around an axis of rotation. Twenty-six different possibilities result when these geometric shapes are permuted with the type of symmetry, and the convex or concave choice of ion milling.

II. SYMMETRY

The geometry of the feature to be ion milled can be classified into two categories based on the choice of reflection in a plane of symmetry or rotation about an axis of symmetry. Any geometry with a curved bottom based on a reflection plane of symmetry in this work will be called a ''trough.'' Any geometry with a curved bottom based on a rotational axis of symmetry will be called either a dome, a dish, or a torus, depending on whether a circle or an annulus is used in the $x-y$ plane and the convex/concave property of the curve involved. The concept of a feature being convex or concave was also established as an ion milling parameter to handle the two possible arrangements of a particular type of cross-section. Physically, convex or concave determines the depth relationship between the center and the outside edge of the feature. The relationship is established with dose: concave

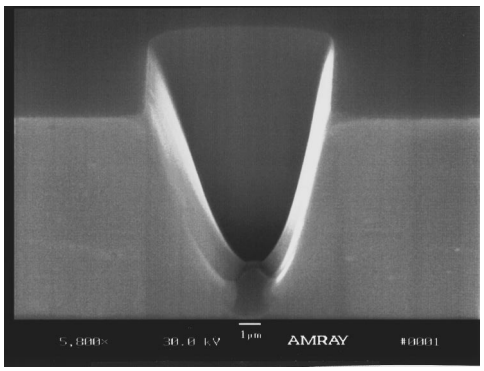

FIG. 4. Perspective and edge views of a parabolic trough ion milled in Si(100), using a 10 μm×5 μm pixel pattern.

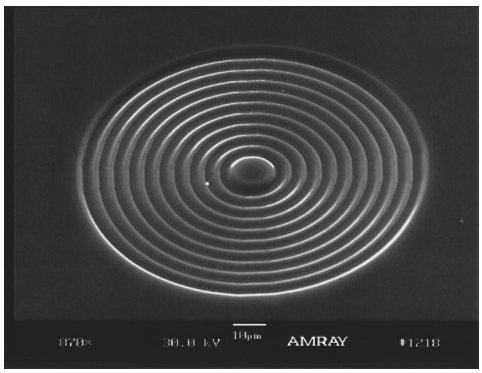

FIG. 6. A 45° SEM perspective view of the rotationally symmetric sine pattern ion milled in Si(100) on the annulus pattern.

requires more dose at the center than at the edges of the feature, while convex requires more dose at the edges of the feature than at center. Therefore, concave and convex features are created by inversion of the ion dose on the $x-y$ milling pattern.

A. Specific examples: Parabolic and sinusoidal cross-sections

A parabolic cross-section will need a focus coefficient, f, and a sinusoidal cross-section will need an amplitude ($0.5H=0.5A\times$length), and a period (n) beside the length for mathematical determination of the pixel dwell time. We begin by noting that we have a pixel array in two dimensions, in which we designate a characteristic length. To determine a parabolic cross-section based on the length, we specify an input parameter p, which relates the maximum depth to the repair length, by the relationship $f=p\times$length. To determine a sinusoidal cross-section, we need two parameters: amplitude ($H/2$) and period number (n). Both can be based on the length, as shown in Figs. 2 and 3.

B. Algorithm generating the dwell time for the curved cross-section geometries

The mathematical expressions for the depth of each of the geometric possibilities were programmed into the ion beam deflection software. In all the program modules for curved cross-section milling, the dwell time per pixel is calculated using the information of the depth relationship dictated by the geometry, the symmetry, and the information in the outlined pattern. It is then written into the ion milling address array, which is used to actuate the machine to work on the pattern for the curved cross-section geometry.

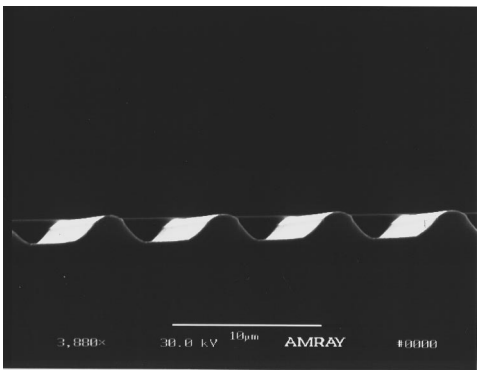

FIG. 5. Edge view of a sinusoidal pattern ion milled in Si(100) on a 60 μm×30 μm pixel pattern.

III. EXPERIMENTAL VERIFICATION

Several representative FIB micromillings were made to verify the algorithm and coding. These are the parabolic trough (parabolic cross-section with a plane of symmetry), a sinusoidal trough, a hemispherical dome, and a sinusoidal annulus pattern.

The pixel dwell times in the cross-section planes (in proportional to the distance to the symmetry axis) are presented in Fig. 2 for the parabolic trough, and in Fig. 3 for one period of the sinusoidal (cosine) trough. Each of these shapes was milled in Si(100) using a 20 keV Ga^+ ion beam with an approximate spot size of 0.4 μm full width at half-maximum (FWHM).

The parabolic trough shown in Fig. 4 was done using a 10 μm×5 μm pixel pattern on a 40 μm field. The resulting shape adheres to a parabolic relationship quite well, but the absolute value of the depth is twice the value expected on the basis of the dose received at the apex. The depth of ion milling versus dose was independently calibrated in Si(100) with constant depth features. Sinusoidal troughs at the edge of a Si(100) slab are shown in Fig. 5. The initial conditions called for a 60 μm×39 μm field containing six periods of a cosine wave, with a wavelength of 10 μm and an expected depth of 2 μm. The edge view in Fig. 5 shows four of the six periods of oscillation, with a depth of 1.7 μm, and a top view SEM shows a wavelength of 10 μm. Note the minimum in the sinusoidal pattern is flat bottomed, a phenomenon also observed also in the parabolic ion milling (Fig. 4).

Rotational symmetry with the sinusoidal pattern is demonstrated in Fig. 6, which starts by outlining an annular pattern. The ID of the annulus is 15 μm with a 115 μm OD, and 10 periods of oscillation between the inner and outer diameter, yielding a sine pattern with a wavelength of 5 μm. Several variations of diameters and periodicity were also ion milled using this basic geometry.

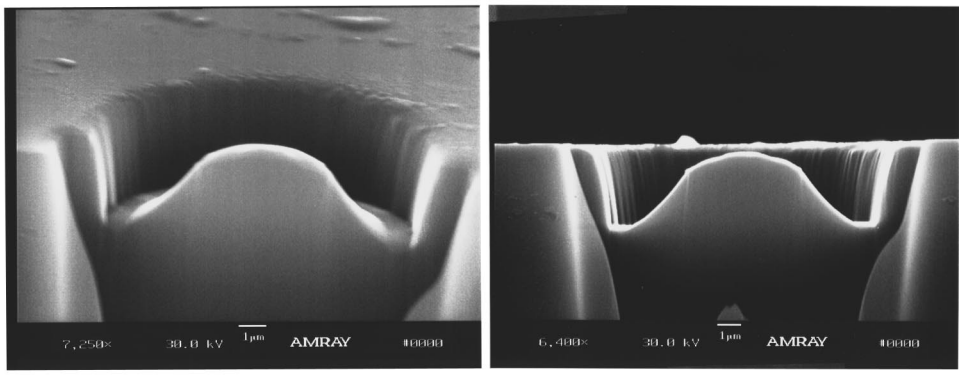

(a) (b)

FIG. 7. (a) A perspective SEM view of a convex dome based on a 15 μm diam circular pattern. (b) An edge SEM view showing the cross-section profile of the convex dome.

A circular dome (convex) shape on a 15 μm diam circular pattern is shown at two scanning electron microscopy viewing angles in Fig. 7. The dome was sectioned to show the profile when tilted to 90°, as in Fig. 7(b). The depth at the periphery of the dome was measured at 3.4 μm, while a depth of 4.5 μm was expected, based on the dose at that point. The cross-section shows that the expected semicircular profile was not obtained, and a small region near the outer diameter has a flat bottom, where a cusp is expected.

IV. DISCUSSION

The experimental results show that the ion beam control programs produces a good first-order approximation to the desired geometries and gives features with depths close to expectation, with the exception of the parabolic cuts. Departures from the exact geometries include steeper descent angles on sidewalls, and some flat-bottomed features where curvature should occur. Apart from the factors already considered in coding (like dose and dwell time) in the program, there are several factors that can significantly affect the final profile in FIB milling under a particular situation. The two major factors are: (1) the relation between the sputter yield and the ion beam incident angle; (2) the effect of step change in dwell time, which is associated with the number of trapezoids used to represent the curve profile. The incremental dose resulting from overlap of the ion beam on adjacent pixels will also distort the geometry.

A. Effect of variable sputter yield at high incident angles

Sputter yield is a material-related property and has a nonconstant relation to the ion beam incident angle with respect to the normal of the substrate surface. According to Yamamura *et al.*,[20] the sputter yield for Si subject to 20 keV Ga^+ bombardment, will reach a peak between 70° and 80° which is about three times that over the range of 0° to 45°, and then drop to 0 at grazing incidence. This phenomenon is significant in our process since most of the curves in this study cover the sharply changing region from 45° to 90°. Consider the angle of incidence variation as the hemispherical dome of Fig. 7 develops. The angle of incidence (with respect to the surface normal) will vary from 0° at the center to $\beta = \arcsin(r/\text{length})$, the final angle of the surface normal under a particular pixel to form a circular curve. Thus, there is a dynamic change of ion beam incidence angle in the process of the curved surface formation. The effect of the changing sputter yield will be incorporated into the surface generation process and the distortion accumulated. The software was, however, developed on the assumption of uniform sputter yield throughout all the surface generating processes, and this accounts for the departures from expected geometry when the angle of incidence is variable as the feature is ion milled.

B. Consequence of pixel size and data type conversion

In the algorithm of depth computation, the pixel distance is represented by integer data type, because pixels (as integer numbers) are used to represent the planar dimension. For curved cross-sections, the computation of depth is made first with real numbers based on the distance dimension in the $x-y$ plane. Then, the real number depth is converted back into the nearest integer number depth which is used to compute the dwell time (also an integer number). Because of this conversion in the algorithm, the differentiable real number depth variation (i.e., depth resolution) is determined by the basic increment/decrement step in the number of pixels over the distance dimension in the $x-y$ plane, i.e., the pixel size. Any numerical variation in real number depth within the depth resolution will be either promoted or demoted into its next integer value.

When the pixel size is large, for a given curved profile, the resolution is coarse, resulting in a poor approximation to the profile; on the other hand, when the pixel size is small, the resolution is fine, resulting in a more accurate approximation to the profile. Thus, the consequence is that we can see a flat line representation for a curve segment having a small slope, such as at the deepest point of the parabolic profile shown in Fig. 2. This effect is responsible for the flat

bottoms observed in the sinusoidal pattern in Fig. 5, and in the parabolic cross-section shown in Fig. 4.

One additional complication when ion milling these geometries is the effect of redeposition. Redeposited material will add to the flat-bottom effect seen at the outer diameter in the convex dome of Fig. 7, and at the apex of the parabolic feature in Fig. 4. The effects of pixel resolution and angle of incidence are dominant effects and can be corrected to some degree, which forms the basis of continuing study; however, the effect of redeposition cannot be avoided, especially in high aspect ratio features.

C. Pixel size versus ion beam diameter

The pixel size is small relative to the ion beam FWHM for all the shapes in this study. The consequence of this is an ''overlap effect'' which exaggerates the dose received in regions of the deflection pattern, which have long dwell times. This problem has been addressed in a separate study,[21] which uses a mathematical model to solve for dwell times needed to produce a cavity of a particular cross-section. The model takes the absolute ion yield and the variation of ion yield as a function of angle of incidence into account, but does not correct for redeposition. The exact solution provided by the mathematical model will be programmed into the ion beam control software in the near future.

[1]L. R. Harriott, *Beam Processing Technologies*, edited by N. G. Einspruch, S. S. Cohen, and R. N. Singh (Academic, San Diego, 1989), Vol. 4, p. 157.
[2]E. C. G. Kirk, R. A. McMahon, J. R. A. Cleaver, and A. Ahmed, J. Vac. Sci. Technol. B **6**, 1940 (1988).
[3]Y. Ochiai, K. Gamo, and S. Namba, J. Vac. Sci. Technol. B **3**, 67 (1985).
[4]Y. Ochiai, J. Vac. Sci. Technol. B **4**, 333 (1986).
[5]L. R. Harriott, J. Vac. Sci. Technol. B **11**, 2012 (1993).
[6]G. Crow, J. Puretz, J. Orloff, R. K. DeFreez, and R. A. Elliott, J. Vac. Sci. Technol. B **6**, 1605 (1988).
[7]T. Ohnishi, Y. Kawanami, and T. Ishitani, Jpn. J. Appl. Phys., Part 2 **29**, 188 (1990).
[8]T. Ishitani, T. Ohnishi, and Y. Kawanami, Jpn. J. Appl. Phys., Part 2 **29**, 2283 (1990).
[9]T. Ishitani, J. Vac. Sci. Technol. B **9**, 2633 (1991).
[10]A. Yamaguchi, M. Shibata, and T. Hashinaga, J. Vac. Sci. Technol. B **11**, 2016 (1993).
[11]M. H. F. Overwijk, F. C. van den Heuvel, and C. W. T. Bulle-Lieuwma, J. Vac. Sci. Technol. B **11**, 2021 (1993).
[12]M. J. Vasile, D. Grigg, J. E. Griffith, E. Fitzgerald, and P. E. Russell, Rev. Sci. Instrum. **62**, 2167 (1991).
[13]J. E. Griffith, D. Grigg, M. J. Vasile, P. E. Russell, and E. A. Fitzgerald, J. Vac. Sci. Technol. A **10**, 694 (1992).
[14]M. J. Vasile, C. J. Biddick, and S. A. Schwalm, J. Vac. Sci. Technol. B **12**, 2388 (1994).
[15]M. J. Vasile, C. J. Biddick, and S. A. Schwalm, *Micromechanical Systems*, edited by A. P. Pisano, J. Jara-Almonte, and W. Trimmer (ASME Press, New York, 1993), p. 81.
[16]C. R. Friedrich and M. J. Vasile, J. Microelectromech. Syst. **5**, 33 (1966).
[17]M. J. Vasile, C. R. Friedrich, B. Kikkeri, and R. McElhannon, J. Precision Engineer. **19**, 180 (1996).
[18]H. Ximen, R. K. DeFreez, J. Orloff, R. A. Elliott, G. A. Evans, N. W. Carlson, M. Lurie, and D. P. Bour, J. Vac. Sci. Technol. B **8**, 1361 (1990).
[19]C. J. Biddick, Bell Labs. Lucent Technologies.
[20]Y. Yamamura, Y. Itikawa, and N. Itoh, Angular Dependence of Sputtering Yields of Monatomic Solids, IPPJ-AM-26, Institute of Plasma Physics, Nagoya University, Nagoya, Japan (1983).
[21]R. Nassar, M. J. Vasile, S. Liu, and W. Zhang, J. Vac. Sci. Technol. A (submitted).